J|A|C|S COMMUNICATIONS

Published on Web 08/03/2009

Selective Attachment of Antibodies to the Edges of Gold Nanostructures for Enhanced Localized Surface Plasmon Resonance Biosensing

Srinivas R. Beeram and Francis P. Zamborini*

Department of Chemistry, University of Louisville, Louisville, Kentucky 40292

Received May 30, 2009; E-mail: f.zamborini@louisville.edu

In this work, we chemically controlled the binding location of anti-immunoglobulin G (anti-IgG) on Au nanostructures and correlated the location determined by atomic force microscopy (AFM) with the visible absorbance spectrum. Correlating the optical properties of metal nanostructures with the site of biomolecule binding is important both fundamentally and for optimum sensing by localized surface plasmon resonance (LSPR) or surface-enhanced Raman spectroscopy (SERS).

When the frequency of incident photons matches that of the collective oscillations of the conduction-band electrons of noble metal nanoparticles, LSPR occurs.[1] The result is a strong absorption band(s) for metals such as Au and Ag in the visible region. The intensity and wavelength of the LSPR band depends on the dielectric properties of the environment surrounding the metal, which has been exploited for biosensing applications.[2] The response is usually a red shift and increased intensity of the band upon analyte binding. LSPR-based biosensing is promising because it is highly sensitive, simple, low cost, and label-free (see the Supporting Information for further background).

Several factors control the LSPR response of metal nanostructures to dielectric changes in the environment, including the size,[3,4] shape,[4] and composition[5] of the nanostructure, proximity to another nanoparticle,[6] and interaction with a substrate.[7] Studies have focused on the sensitivity to global changes in the refractive index (RI) of the entire medium surrounding the metal nanostructures or to local changes associated with direct molecular or biomolecular binding. Predictions generally show that the RI sensitivity increases as the bulk LSPR band moves to higher wavelengths.[8,9] Chen et al.[4] showed this experimentally, as the RI sensitivity of Au nanostructures followed the order branches > bipyramids > rods > cubes > spheres. The sensitivity to local binding of molecules decreases exponentially with increasing distance within 40−50 nm from the nanostructure and increases with increasing analyte volume.[10] The global RI sensitivity serves as an upper limit to the local response.[9] It is also predicted that the sensitivity depends on the molecule binding location on the metal nanostructure. Van Duyne and co-workers[7a] predicted that sharp regions of a nanostructure act as "hot spots", being very sensitive to local dielectric changes, while flat terraces are comparably less sensitive. There are few experimental examples supporting this. Van Duyne and co-workers[11] showed large shifts in the LSPR band for triangular Ag nanostructures upon nonspecific adsorption of antibodies onto the Cr adhesion layer near the edges, and Sannomiya et al.[12] reported varied responses of an individual Au nanoparticle upon single binding events of smaller nanoparticles via DNA hybridization; this result was partly attributed to different binding locations. While the existence of sharp edges is often used to explain different LSPR sensitivities for differently shaped nanoparticles, there have been no reports demonstrating controlled binding of analyte to the edge regions of metal nanostructures or providing detailed characterization of the binding location.

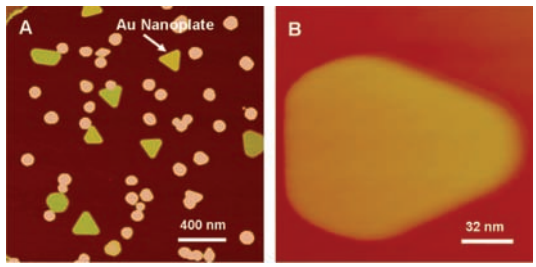

Figure 1. (A) AFM image of Au nanoplates and other nanostructures grown on a silicon surface. (B) Expanded image of an Au nanoplate.

We synthesized Au nanostructures directly on glass and silicon surfaces by a seed-mediated growth procedure (for details, see the Supporting Information).[13] Figure 1 shows an AFM image of a typical silicon sample, which consisted of Au nanoparticles (67%) and triangular, hexagonal, or circular Au nanoplates (33%) in the range of 100−200 nm on a side. We covalently attached anti-IgG to the Au nanostructures by three methods. In the first method, termed "pure MUA", the sample was placed in a 1 mM ethanol solution of mercaptoundecanoic acid (MUA) for 12−15 h, rinsed thoroughly with ethanol, dried under N_2, and then placed in an aqueous solution of 2 mM 1-ethyl-3-(3-dimethylaminopropyl) carbodiimide (EDC) and 5 mM *N*-hydroxy succinimide (NHS) for 1 h. After the sample was rinsed with water and dried under N_2, it was placed in an aqueous 0.029 or 0.29 μg/mL human anti-IgG solution for 12−15 h, rinsed with phosphate-buffered saline and water, and dried under N_2. The second method, termed "10% MUA", involved the same procedure except that we placed the sample into an ethanol solution containing a 1:10 molar ratio (total concentration 1 mM) of MUA and mercaptoethanol (ME) prior to anti-IgG coupling. We called this "10% MUA" because of the solution composition, but the monolayer composition is likely different. In the third procedure, termed "place-exchange", we placed the sample in a 1 mM ethanol solution of ME overnight and then exchanged the ME monolayer with MUA by placing the sample into a 5 mM ethanol solution of MUA for 4 h. Finally, we attached anti-IgG via EDC and NHS coupling. We hypothesized that the place-exchange strategy would lead to selective edge functionalization in view of the results of Murray and co-workers,[14] who speculated that thiol place-exchange reactions on Au nanoparticles occur preferentially at vertex and edge sites because of lessened steric hindrance there. If this is true, the MUA molecules should exchange at edge and vertex sites on the Au nanoplates and nanoparticles, subsequently leading to the attachment of anti-IgG at these sites. (See Schemes S1 and S2 in the Supporting Information for more details concerning anti-IgG attachment).

Figure 2 shows AFM images of Au nanoplates functionalized using the three strategies at the two different anti-IgG concentrations of 0.29 and 0.029 μg/mL. We focused on Au nanoplates because they are atomically smooth and allow easy visualization of anti-

10.1021/ja904387j CCC: $40.75

IgG on the surface. In contrast, we could not identify anti-IgG on the highly curved spherical nanoparticles by AFM. We assume that the coverage and location of anti-IgG on the Au nanoplates reflects that on the spherical nanoparticles. We assigned the bright spots on the nanoplates in Figure 2 to the attached anti-IgG. For the pure MUA strategy (Figure 2A,B), the coverage decreased as the concentration of anti-IgG decreased. This also occurred for the 10% MUA strategy (Figure 2C,D), but the coverages at both concentrations were lower than those for pure MUA because of the smaller number of binding sites on the surface. At 0.029 μg/mL, the 10% MUA surface did not show any bound anti-IgG. With both strategies, the anti-IgG bound randomly to the flat terrace sites of the nanoplates. In contrast, for the place-exchange sample (Figure 2E,F), the anti-IgG attached preferentially at the edges and even the vertex (Figure 2F) of the Au nanoplates. The coverage did not correlate well with the anti-IgG concentration, as shown by a comparison of the 0.29 and 0.029 μg/mL data, suggesting that it was limited by the amount of MUA exchanged on the edge. While only two images are shown in Figure 2, edge localization occurred for 19 out of 22 nanoplates imaged at the two concentrations (see Figures S1 and S2 for AFM images of other nanoplates). As further evidence that selective edge functionalization occurred, increasing the MUA concentration to 6 mM during the place-exchange reaction led to more anti-IgG on the edge sites, as shown in Figure 2G,H (also see Figure S3). We measured the root-mean-square (rms) roughness of the Au nanoplates as a function of anti-IgG concentration (Figure S4) to quantify the surface coverage of anti-IgG for the three strategies. The pure MUA strategy had the largest anti-IgG coverage since it had the largest number of MUA binding sites.

We used a Varian Cary 50 Bio UV−vis spectrophotometer to monitor the absorbance in air (in transmission mode) of the Au nanostructures grown on glass substrates before and after attachment of anti-IgG by the three different strategies. Figure 3 shows the visible spectra of samples of Au nanostructures functionalized by the (A, B) pure MUA, (C, D) 10% MUA, and (E, F) place-exchange methods before and after attachment of anti-IgG from 0.29 and 0.029 μg/mL concentrations (see Figures S5−S13 for all samples). Each sample displayed a major LSPR band between 530 and 550 nm attributed to the Au nanostructures (mainly spherical nanoparticles). We normalized each pair of spectra to the absorbance at the wavelength of maximum absorbance (λ_{max}) before anti-IgG attachment, which made the absorbance at λ_{max} equal to 1.0 before anti-IgG attachment and allowed easy comparison of the relative absorbance increase after anti-IgG attachment for each strategy. Qualitatively, for the pure MUA and 10% MUA samples, there was no significant increase in the LSPR intensity or wavelength due to binding of anti-IgG from the 0.29 and 0.029 μg/mL solutions; the absorbance actually decreased in two out of the four cases. In contrast, there was a significant increase in the intensity and λ_{max} upon binding of anti-IgG from both the 0.29 and 0.029 μg/mL solutions for the place-exchange samples. On the basis of the AFM images, we believe this is due to anti-IgG being located at edge or vertex sites for the place-exchange samples. Even though the anti-IgG coverage is comparably larger for pure MUA at both concentrations and 10% MUA at 0.29 μg/mL, the optical response is insignificant because the anti-IgG is located on the less sensitive terraces. This qualitatively confirms that the LSPR response of Au nanostructures is more sensitive to dielectric changes (analyte binding) on edge sites than on terrace sites. The Van Duyne group previously calculated that an Ag nanotriangle could be less than 10% covered but still exhibit almost its maximum shift if the adsorbate is confined to the edges.[7a]

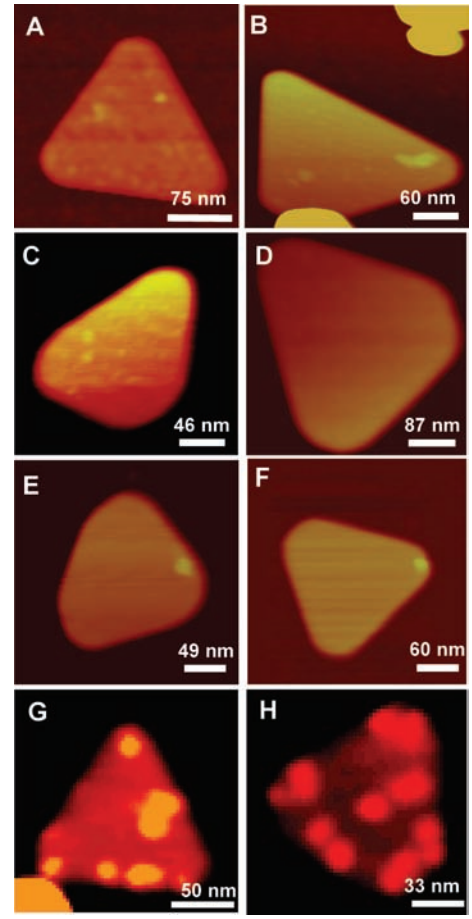

Figure 2. AFM images of Au nanoplates functionalized with anti-IgG using the (A, B) pure MUA, (C, D) 10% MUA, and (E−H) place-exchange strategies with anti-IgG concentrations of (A, C, E, G) 0.29 and (B, D, F, H) 0.029 μg/mL. Place-exchange was performed with (E, F) 5 and (G, H) 6 mM MUA.

Figure 4 shows a quantitative statistical analysis of the change in λ_{max} ($\Delta\lambda_{max}$) and the change in normalized absorbance ($\Delta A/A_{initial}$) as a function of the two anti-IgG concentrations for the three different functionalization strategies and for Au functionalized with ME only as a control (see Tables S1 and S2 for all data). ΔA is equal to $A_{final} - A_{initial}$, where $A_{initial}$ and A_{final} are the absorbances at λ_{max} before and after anti-IgG binding, respectively. The bar graphs show the average and standard deviation measured using three samples for each strategy (two for pure ME). We performed the measurements by marking the samples and monitoring the same area of the glass slide before and after anti-IgG binding. The deviations in $\Delta\lambda_{max}$ and normalized $\Delta A/A_{initial}$ on an untreated sample over a one-week period were at most 2 nm and 0.02 (2%), respectively. Signals in Figure 4 that are equal to or less than these values are therefore insignificant. Figure 4 shows that $\Delta\lambda_{max}$ and $\Delta A/A_{initial}$ were not significant or decreased for the pure MUA, 10% MUA, and ME samples at both concentrations. The decrease in $\Delta A/A_{initial}$ in some cases was due to loss of Au from the slide during soaking in anti-IgG. In contrast, the 5 mM place-exchange samples showed a significant positive $\Delta\lambda_{max}$ of 5−6 nm and a $\Delta A/A_{initial}$ greater than 0.10 (10%) at both concentrations. The 6 mM MUA exchange samples showed an even larger $\Delta\lambda_{max}$ of 9−10 nm for the 0.29 μg/mL concentration (no data at 0.029 μg/mL), consistent with the AFM images showing more anti-IgG on the edges (Figure 2G,H). The $\Delta A/A_{initial}$ was not consistent with this at 6 mM, likely because decrease due to the unpredictable amount of Au lost from the surface during soaking competes with the absorbance increase

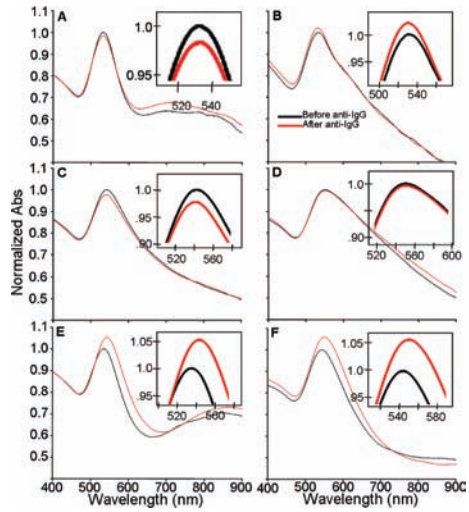

Figure 3. Visible spectra of Au nanostructures functionalized with the (A, B) pure MUA, (C, D) 10% MUA, and (E, F) place-exchange strategies (black) before and (red) after attachment of anti-IgG at concentrations of (A, C, E) 0.29 and (B, D, F) 0.029 μg/mL. The insets show magnified views of the peaks.

due to anti-IgG binding. Regardless, these results clearly indicate that the place-exchange method leads to Au nanostructures that are significantly more sensitive to anti-IgG binding.

Since the Au nanoplates occupy only ~33% of the surface, spherical nanoparticles dominate the visible spectrum, especially at 530−550 nm. We believe the AFM images of Au nanoplates can still explain the optical results because they likely reflect the coverage and location of anti-IgG on the spherical particles, which are known to have well-defined geometries with edge and vertex sites.[14] The edge sites are likely to be more sensitive for all nanoparticle shapes. We also note that the place-exchange samples often exhibited a positive baseline shift upon binding of anti-IgG for some of the samples (Figure 3F and Figures S11−S13), showing that the absorbance increased in spectral regions outside the LSPR band. This baseline shift is a real effect of anti-IgG binding[15] and not a baseline-correction issue. All of the samples were referenced to bare glass. In the 16 samples that were not sensitive to anti-IgG (pure MUA, 10% MUA, and ME), the baseline did not increase significantly, while eight out of the nine place-exchange samples did show an increase, indicating that this is a real effect of anti-IgG binding for those samples.

In summary, we selectively functionalized edge and vertex sites of Au nanostructures with anti-IgG, confirming the location of thiol place-exchange on nanoparticle surfaces. We also showed experimentally that the LSPR response ($\Delta\lambda_{max}$ and $\Delta A/A_{initial}$) is significantly more sensitive to anti-IgG binding on metal nanoparticle

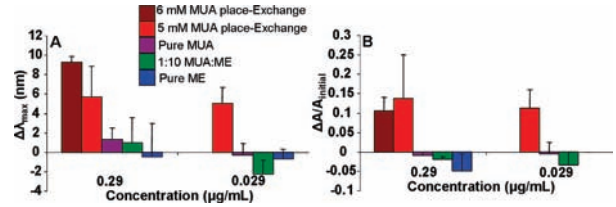

Figure 4. Bar graphs of (A) $\Delta\lambda_{max}$ and (B) $\Delta A/A_{initial}$ for the two anti-IgG concentrations using the three different strategies and ME only.

edge and vertex sites than on terrace sites. Finally, we used the 5 mM place-exchange anti-IgG (0.29 μg/mL) Au samples to detect IgG down to a concentration of 0.1 ng/mL, or ~7 pM (see Figure S14). This is at least 500 times lower than that detected using the pure MUA or 10% MUA samples at 2.9 μg/mL anti-IgG concentration and is comparable to the lowest detection limits of 100 pM and <1 pM reported for streptavidin using Au nanorods[16] and triangular Ag nanoparticles,[17] respectively.

Acknowledgment. We gratefully acknowledge the National Science Foundation (CHE-0518561) for financial support of this research.

Supporting Information Available: More complete background on LSPR sensing, experimental details and schemes, rms measurements, data tables, AFM images, visible spectra, and IgG detection. This material is available free of charge via the Internet at http://pubs.acs.org.

References

(1) Stewart, M. E.; Anderton, C. R.; Thompson, L. B.; Maria, J.; Gray, S. K.; Rogers, J. A.; Nuzzo, R. G. *Chem. Rev.* **2008**, *108*, 494.
(2) Anker, J. N.; Hall, W. P.; Lyandres, O.; Shah, N. C.; Zhao, J.; Van Duyne, R. P. *Nat. Mater.* **2008**, *7*, 442.
(3) Nath, N.; Chilkoti, A. *Anal. Chem.* **2004**, *76*, 5370.
(4) Chen, H.; Kou, X.; Yang, Z.; Ni, W.; Wang, J. *Langmuir* **2008**, *24*, 5233.
(5) Zhang, K.; Xiang, Y.; Wu, X.; Feng, L.; He, W.; Liu, J.; Zhou, W.; Xie, S. *Langmuir* **2009**, *25*, 1162.
(6) Jain, P. K.; El-Sayed, M. A. *Nano Lett.* **2008**, *8*, 4347.
(7) (a) Haes, A. J.; Zou, S.; Schatz, G. C.; Van Duyne, R. P. *J. Phys. Chem. B* **2004**, *108*, 6961. (b) Dmitriev, A.; Hagglund, C.; Chen, S.; Fredriksson, H.; Pakizeh, T.; Kall, M.; Sutherland, D. S. *Nano Lett.* **2008**, *8*, 3893.
(8) Lee, K.-S.; El-Sayed, M. A. *J. Phys. Chem. B* **2006**, *110*, 19220.
(9) Miller, M. M.; Lazarides, A. A. *J. Phys. Chem. B* **2005**, *109*, 21556.
(10) Nusz, G. J.; Curry, A. C.; Marinakos, S. M.; Wax, A.; Chilkoti, A. *ACS Nano* **2009**, *3*, 795.
(11) Haes, A. J.; Hall, W. P.; Chang, L.; Klein, W. L.; Van Duyne, R. P. *Nano Lett.* **2004**, *4*, 1029.
(12) Sannomiya, T.; Hafner, C.; Voros, J. *Nano Lett.* **2008**, *8*, 3450.
(13) (a) Wei, Z.; Mieszawska, A. J.; Zamborini, F. P. *Langmuir* **2004**, *20*, 4322. (b) Mieszawska, A. J.; Zamborini, F. P. *Chem. Mater.* **2005**, *17*, 3415.
(14) Hostetler, M. J.; Templeton, A. C.; Murray, R. W. *Langmuir* **1999**, *15*, 3782.
(15) Bendikov, T. A.; Rabinkov, A.; Karakouz, T.; Vaskevich, A.; Rubinstein, I. *Anal. Chem.* **2008**, *80*, 7487.
(16) Marinakos, S. M.; Chen, S.; Chilkoti, A. *Anal. Chem.* **2007**, *79*, 5278.
(17) Haes, A. J.; Van Duyne, R. P. *J. Am. Chem. Soc.* **2002**, *124*, 10596.

JA904387J